



September 17, 2001

U.S. Nuclear Regulatory Commission  
ATTN: Document Control Desk  
Washington, DC 20555-0001

**DOCKET 50-255 - LICENSE DPR-20 - PALISADES PLANT**  
SUPPLEMENTAL INFORMATION FOR REQUEST FOR APPROVAL TO USE ASME  
CODE CASE N-504-1 FOR REPAIR OF CONTROL ROD DRIVE MECHANISM  
UPPER HOUSING ASSEMBLIES – (RELIEF REQUEST RR-15)

On July 30, 2001, Nuclear Management Company, LLC (NMC) submitted a request for NRC approval to use ASME Code Case N-504-1 for the repair of control rod drive mechanism (CRDM) upper housing assemblies. Discussion with NRC Staff identified that it would be appropriate that the submittal take the form of a Relief Request. Enclosure 1 provides the relief request for the use of Code Case N-504-1. Staff also had a concern regarding the possible propagation of cracks into the weld overlay repairs. Enclosure 2 provides discussion addressing this concern. Finally, Staff suggested that the commitment regarding submittal of a plan for future inspections of weld overlay repairs should be clarified. This letter provides that clarification.

Prompt NRC review and approval are requested.

SUMMARY OF COMMITMENTS

This letter contains no new commitments and revises the one commitment made in our July 30, 2001 letter on this subject. The previous commitment was:

Following completion of any weld overlay repairs made in accordance with this request, NMC will provide the NRC with its plan for future inspections of the repaired housings.

The revised commitment is:

In each future refueling outage, until such time as repaired CRDM upper housings are replaced, at least 10% of those housings for which weld overlay has been applied, but no fewer than 3 CRDM housings, will be inspected. The

A047

inspection shall consist of radiographic and ultrasonic testing, at a minimum, to ensure the integrity of the overlay and detect any unexpected crack propagation.

A handwritten signature in black ink, appearing to read "Paul A. Harden". The signature is fluid and cursive, with a large initial "P" and "H".

Paul A. Harden  
Director, Engineering

CC Administrator, Region III, USNRC  
Project Manager, NRR, USNRC  
NRC Resident Inspector – Palisades

Enclosures

**ENCLOSURE 1**

**NUCLEAR MANAGEMENT COMPANY, LLC  
PALISADES PLANT  
DOCKET 50-255**

**SEPTEMBER 17, 2001**

**SUPPLEMENTAL INFORMATION FOR  
REQUEST FOR APPROVAL TO USE ASME CODE CASE N-504-1 FOR REPAIR OF  
CONTROL ROD DRIVE MECHANISM UPPER HOUSING ASSEMBLIES**

**RELIEF REQUEST RR-15**

## **RELIEF REQUEST NUMBER – RR-15**

### **COMPONENT IDENTIFICATION**

Code Class	1
Code Reference	IWA-4120
Examination Category	B-O
Item Number	B14.10
Component Description	Control Rod Drive Upper Housing

### **CODE REQUIREMENT**

ASME Section XI Article IWA-4120 requires repairs to be performed in accordance with the Owner's Design Specification and the original Construction Code of the component or system. Later Editions and Addenda of the Construction Code or of Section III, either in their entirety or portions thereof, and Code Cases may be used.

### **BASIS FOR RELIEF**

ASME Section XI Article IWA-4120 allows repairs to be made in accordance with Code Cases. American Society of Mechanical Engineers (ASME) Code Case N-504-1, "Alternate Rules For Repair of Class 1, 2, and 3 Austenitic Stainless Steel Piping, Section XI, Division 1," was approved by the ASME Boiler and Pressure Vessel Code (B&PV Code), Section XI on April 30, 1992, and was revised (N-504-1) on August 9, 1993. This Code Case expired on July 1, 1995 with the publication of ASME Section XI, 1995 Edition. However this code case remains listed as an acceptable code case in the latest edition of Regulatory Guide 1.147, "Inservice Inspection Code Case Acceptability, ASME Section XI Division 1," Revision 12, dated May 1999. This Code Case is written for application on piping components. While not considered a piping component, the CRDM upper housing assemblies are assembled using standard flanges, eccentric reducers and piping. After assembly the housings are machined to manufacturer's specifications. Materials and methods of welding are consistent with direct application of the code case. Therefore, pursuant to 10 CFR 50.55a(a)(3)(i) and footnote 6 of 10 CFR 50.55a, Nuclear Management Company (NMC) requests relief for the use of Code Case N-504-1 for the repair of any Control Rod Drive Mechanism Upper Housing Assemblies for which the Code Case can be shown to apply, and where such repair is determined to be the

appropriate course of action. Code Case N-504-1 provides an acceptable alternative repair to the repair techniques presently approved for use by the NRC.

APPLICABLE TIME PERIOD

Relief is requested for the third ten-year interval of the Inservice Inspection Program for Palisades.

**ENCLOSURE 2**

**NUCLEAR MANAGEMENT COMPANY, LLC  
PALISADES PLANT  
DOCKET 50-255**

**SEPTEMBER 17, 2001**

**SUPPLEMENTAL INFORMATION FOR  
REQUEST FOR APPROVAL TO USE ASME CODE CASE N-504-1 FOR REPAIR OF  
CONTROL ROD DRIVE MECHANISM UPPER HOUSING ASSEMBLIES**

**DISCUSSION REGARDING CRACK PROPAGATION  
INTO THE WELD OVERLAY**

25 Pages



August 29, 2001  
SIR-01-087, Rev. 2  
BMG-01-010

3315 Almaden Expressway  
Suite 24  
San Jose, CA 95118-1557  
Phone: 408-978-8200  
Fax: 408-978-8964  
www.structint.com  
bgordon@structint.com

Mr. Robert Van Wagner  
Consumers Energy  
Palisades Nuclear Plant  
27780 Blue Star Memorial Hwy.  
Covert, Michigan 49043-9530

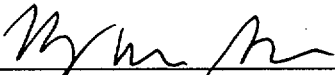
Subject: Stress Corrosion Cracking Evaluation of the Type 309L Stainless Steel Weld  
Overlays for Palisades

Dear Mr. Van Wagner,

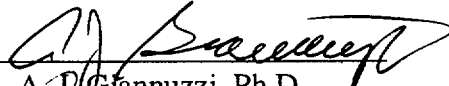
This letter report is a description and an evaluation of the stress corrosion cracking (SCC) propensities of duplex and austenitic stainless steels in aqueous environments as related to the planned Type 309L stainless steel weld overlay of control rod drive mechanism (CRDM) reactor coolant pressure boundary welds. More specifically, this letter report provides:

1. An evaluation of the propensity for SCC initiation in the weld overlay.
2. An evaluation of the propensity for SCC propagation into the weld overlay.
3. An evaluation of the residual stress profile in the weld overlay.

We thank you for the opportunity to provide this report to Nuclear Management Company. If you have any questions on the content of this letter report, please do not hesitate to contact Tony or me.

Prepared by:   
B. M. Gordon, P.E.

Date: 8/28/01

Reviewed by:   
A. D. Giannuzzi, Ph.D.

Date: 8/29/01

Approved by:   
M.L. Herrera, P.E.

Date: 8/29/01

rp  
Attachment  
cc: W-CPC-13Q-2

# STRESS CORROSION CRACKING EVALUATION OF THE TYPE 309L STAINLESS STEEL WELD OVERLAYS FOR PALISADES

## 1.0 Introduction and Summary

Wrought austenitic stainless steels are susceptible to both intergranular stress corrosion cracking (IGSCC) and transgranular stress corrosion cracking (TGSCC) in aqueous environments as a function of the material's microstructure and the environment's constituents. Historically, the threshold for chloride stress corrosion cracking (CSCC) has been identified as 140 °F (60 °C) (1). More recent data indicates that the threshold can occur at lower temperatures depending upon the dissolved oxygen and chloride concentration present, and the condition of the alloy, i.e., whether the material has received a sensitizing heat treatment, thus favoring IGSCC.

This letter report describes the crack initiation and crack propagation SCC propensities of duplex and austenitic stainless steels in aqueous environments as related to the planned Type 309L stainless steel weld overlay of control rod drive mechanism (CRDM) reactor coolant pressure boundary welds.

Section 2.0 and Section 3.0 discuss the crack initiation and crack propagation propensities of Type 309L stainless steel in the Palisades CRDM environment, respectively. These two analyses are based on the available materials and water chemistry information plus the application of a fundamental crack growth rate model. The results of these two sections of the report demonstrate that crack initiation is unlikely and crack propagation is at least an order of magnitude slower than Type 304 stainless steel.

Section 7.0 provides an analysis of the residual stress profile for the weld overlay. It is shown that the weld overlay provides some compressive residual stress benefit in the region between the weld and the shoulder area. The compressive residual stress reduces the driving force for new SCC initiation and propagation for cracks after the weld overlay is applied. Also, the weld overlay material is not expected to be exposed to the primary coolant based upon the expected driving force demonstrated by the analysis in this report.

Therefore, consistent with the NRC philosophy of the application of two fundamental remedies for the mitigation of SCC, the proposed Type 309L stainless steel weld overlay does indeed address two of the three required parameters for SCC, i.e., susceptible material and tensile stress. The synergistic combination of these factors clearly indicate that the planned Type 309L stainless steel weld overlay can be considered as a permanent repair for the CRDMs at Palisades.

## 2.0 CSCC Initiation of Type 309L Stainless Steel

Figure 1 presents the cracking threshold for both TGSCC and IGSCC of austenitic stainless steels as a function of oxygen and chloride concentration at 480-570 °F, the temperature range of interest at Palisades (2). One observes from this figure that at oxygen levels of 100 to 200 ppb, cracking in sensitized stainless steels can occur in extremely dilute chloride solutions (as low as 10 ppb). In fact, IGSCC of sensitized Type 304 stainless steel can occur in high temperature oxygenated water with no chloride and the theoretically lowest possible conductivity of 0.055

$\mu\text{S}/\text{cm}$ . On the other hand, this figure reveals that a concentration of approximately 10,000 ppb (10 ppm), chloride is required for TGSCC to initiate in non-sensitized austenitic stainless steel. The cracking in the sensitized stainless steel is intergranular whereas the cracking in the annealed material is transgranular. It is further noteworthy that, if no oxygen is present, no CSCC occurs, independent of the chloride concentration, since it is the required reduction of oxygen to the hydroxyl ion that is involved in the corrosion reaction. The chloride anion role in the corrosion reaction is to enhance the conductivity of the electrolyte and degrade the passive film on the stainless steel surface.

The situation for duplex stainless steels is quite different. Figure 2 presents results for 18 Cr (Types 304 and 316 stainless steel) and 22 Cr duplex (2205) stainless steels, comparing the CSCC resistance of these alloys to wrought austenitic stainless steels in aqueous environments as a function of temperature (1). One should note that the 22 Cr duplex stainless steels have a similar composition to that of Type 309L stainless steel and are, therefore, representative of this alloy. Calculations reveal that Type 309L stainless steel weld metal and duplex 2205 stainless steel have nearly equal Cr equivalent values at 26.1 and 28.5, respectively, Table 1 (3). Type 304 stainless steel has a lower Cr equivalent of 21.

One notes that for these alloys, the threshold for CSCC occurs at approximately 400 °F (200 °C) and at concentrations of approximately 10 ppm chloride for the 18 Cr alloy and 1000 ppm for the 22 Cr alloy. Thus, it is observed that the CSCC resistance of austenitic stainless steels dramatically improves as a function of temperature and chloride concentration with the addition of ferrite and chromium in the alloy.

Figure 3 presents additional data on the CSCC of stainless steels in neutral chloride environments with 8 ppm dissolved oxygen at applied stresses that exceed the respective yield strength of the materials (4). Again, duplex alloy 2205 is dramatically more resistant to CSCC compared to Types 304 and 316 stainless steels. As noted above, a similar CSCC response would be anticipated for Type 309L stainless steel.

The failure mode in chlorides is TGSCC for non-sensitized austenitic stainless steel. However, if the stainless steel is sensitized, the cracking can be either transgranular or intergranular or mixed mode. One investigator reported that the cracking mode of Type 304 stainless steel U-bend specimens shifted from transgranular to intergranular if the steel were severely sensitized (5). When sensitized, the IGSCC was much more extensive and failure occurred in much shorter times than comparative annealed samples which were forced to crack by TGSCC. All samples were tested in aqueous solutions between 165 and 200 °F (74 and 93 °C) and at chloride levels as low as 5 ppm. Cracking occurred when the pH was neutral, but was absent when the pH was alkaline. The authors of this review report have shown that austenitic alloys containing small amounts of ferrite (greater than 10%) were immune to cracking in the low-temperature, neutral chloride solutions (3). These alloys include Type 308L stainless steel weld metal, cast Type 304L stainless steel (CF3), Type 329 stainless steel and Uranus 50 duplex stainless steels.

Based upon these results, one observes that the CSCC initiation susceptibility of austenitic stainless steels is extremely dependent upon material condition, dissolved oxygen content and temperature.

The most prudent method of addressing the CSCC initiation issue is to use the factor of improvement (FOI) methodology that has been utilized by the BWRVIP and has been accepted by the NRC (6). For example, a comparative SCC study in the most aggressive 42% magnesium chloride solution at 310 °F (154 °C) on annealed Type 304 stainless steel (0.071% C) and a laboratory heat of a 12% ferrite duplex stainless steel (0.064 %C, 20.25% Cr and 8.54% Ni,  $Cr_{eq} = 21.5$ ) revealed a FOI of 19 based on respective times to cracking (7). That is, it took almost twenty times longer to initiate CSCC in the duplex alloy in this very aggressive environment. It is anticipated that Type 309L stainless steel with its higher Cr content, higher Ni content and percent ferrite (13%) that is to be applied as a weld overlay at Palisades would produce an even greater FOI than this experimental heat.

### 3.0 CSCC Propagation of Type 309L Stainless Steel

There has been some discussion on the relative crack propagation rates for IGSCC and TGSCC. Since IGSCC propagates through the higher energy grain boundaries, it would be fundamentally expected that IGSCC propagation would be more rapid. A corrosion engineering “rule of thumb” is a factor of three slower for TGSCC versus IGSCC propagation. In the specific case of the Fort Calhoun CRDM housing cracking, a literature survey revealed that the TGSCC growth rate of Type 347/348 stainless steel was three to ten times slower than the equivalent IGSCC growth rate (8-10).

Figure 4 presents a schematic of the relative crack propagation rates for IGSCC and TGSCC as a function of the crack tip strain rate (11). At lower crack tip strain rates, which would be anticipated for real world components, IGSCC propagation is more rapid than TGSCC. This difference in crack growth rate was noted for the Fort Calhoun CRDM cracking analysis.

Unfortunately, there are no published data on the relative crack propagation rates of duplex stainless steel in dilute chlorinated environments. Therefore, the crack growth rate of Type 309L stainless steel in dilute chlorinated environments must be evaluated based on other materials data.

The approach for calculating the relative Type 309L stainless steel crack growth rates is based on the application of the deterministic film-rupture/slip-oxidation model (12 - 16). This model has been reviewed and accepted by the BWRVIP for use in evaluating the impact of water chemistry variables on crack growth rate in stainless steels over the electrochemical corrosion potential (ECP) range of -500 to 200 mV(SHE) and for conductivities up to 1  $\mu$ S/cm (e.g., 260 ppb Cl<sup>-</sup>, 170 ppb Na<sup>+</sup>). It also has been accepted by the Ministry of Economy, Trade and Industry (METI, formally MITI) in Japan.

The film-rupture/slip-oxidation crack propagation rate/crack tip strain rate relationship may be generalized by:

$$\bar{V}_t = A \dot{\epsilon}_{ct}^n$$

where  $\bar{V}_t$  is the average environmentally controlled crack propagation rate,  $\dot{\epsilon}_{ct}$  is the crack tip strain rate, and A and n are constants depending on the material and environment compositions at the crack tip. There are limits to the validity of this relationship, however, which are observed at

high and low crack tip strain rates. At low crack tip strain rates, the ultimate criterion is that sharp cracks cannot be maintained when the average crack tip propagation rate,  $\bar{V}_t$ , approaches the oxidation rate on the crack sides,  $V_s$ . Under these conditions, therefore, the crack propagation rate will slow down with exposure time and crack arrest will eventually occur due to blunting. At high crack tip strain rates, ( $\sim 10^{-2}/s$ ), a bare surface is continuously maintained at the crack tip, and the environmentally controlled crack propagation rate becomes independent of  $\dot{\epsilon}_{ct}$ , since it cannot exceed the Faradaic equivalent of the bare surface dissolution rate.

Variables in the film-rupture/slip-oxidation crack growth model include material type, degree of sensitization, stress intensity, ECP, conductivity and irradiation. The film-rupture/slip-oxidation model predicts the expected rate of actively growing cracks; it is not a mean or a bound of SCC data. A comparison of highly accurate laboratory crack growth rate measurements using the reversing DC potential drop technique (PDT) and film-rupture/slip-oxidation model predictions indicates that the film-rupture/slip-oxidation model is conservative, i.e., crack growth rate will be over estimated. As intended, film-rupture/slip-oxidation calculations represent the high end of the crack growth data within a factor of 2 for approximately 95% of the data.

Highly susceptible weld sensitized Type 304 stainless steel in a highly oxidizing environment (ECP = 0 mV(SHE), i.e.,  $\sim 500$  ppb dissolved oxygen) was used as the reference material and environment, respectively. The film-rupture/slip-oxidation model was used to develop an IGSCC crack growth rate curve as a function of conductivity/chloride concentration, Figure 5.

This IGSCC Type 304 stainless steel crack growth rate curve was reduced by a factor of three to create a curve representing the TGSCC of Type 304 stainless steel. This crack growth rate curve was subsequently reduced by a factor of 7.8 to reflect the inherit SCC resistance of Type 309L stainless steel over Type 304 stainless steel based on the film-rupture/slip-oxidation crack growth model comparison between annealed and weld sensitized Type 304 stainless steel. Thus, the crack growth rate FOI of Type 309L stainless steel over weld sensitized Type 304 stainless steel is approximately 24.

Figure 5 also contains crack growth rate points for Type 304 stainless steel in highly chlorinated lower temperature environments (17) plus the estimated Fort Calhoun CRDM crack growth rate point (8). Since the two high chloride points in 200 °F (93 °C) water in 22% NaCl and 42% MgCl<sub>2</sub> contain  $1.4 \times 10^8$  and  $3.1 \times 10^8$  ppb chloride, respectively, run-out arrows are required. Although characterized by a lower temperature, i.e., 200 °F (93 °C) versus 550 °F (288 °C), the dramatically higher chloride concentration crack growth rates are consistent with the modeling results.

The derivation of the Fort Calhoun crack growth rate data point is discussed in Section 5.0 (8). It was estimated that the dissolved oxygen in the Fort Calhoun CRDM was 300 to 1300 ppm as compared to the 500 ppb dissolved oxygen used in the model calculations. The chloride content was conservatively estimated at the Fort Calhoun chloride technical specification limit of 150 ppb.

## 5.0 Relevant Field Experience

A leak was detected in one of the two spare inactive Type 348 stainless steel CRDMs (a.k.a. control element drive mechanism [CEDM]) upper housings on the reactor closure head after seventeen years of operation of Fort Calhoun (8). The axially oriented through-wall crack was in the vicinity of a weld overlay area on the housing. The cause of the cracking was concluded to be TGSCC produced by a stagnant oxygenated (330 to 1300 ppm) environment and a high residual stress at 400 °F (204 °C). In contrast, active, vented CRDM housings have dissolved oxygen concentrations of only approximately 5 ppb. The fracture surface, as evaluated by scanning electron microscopy (SEM), featured well-defined concentric rings.

A literature survey performed by the Fort Calhoun engineering staff after the crack was identified indicated a TGSCC propagation rate of  $1.42 \times 10^{-5}$  in/h for Types 347 and 348 stainless steels (8). When this rate was applied to the housing wall thickness of 18 mm, the time from crack initiation to failure was determined to be 2,000 days. Thus, by counting back 2,000 reactor operating days from the time when the leak was discovered (December 1990), the date of crack initiation could be estimated. The crack initiation date was determined by this method to be August 1983. This date was in excellent agreement with the general time period obtained by counting fracture surface concentric rings. In turn, these results supported the crack growth rate for TGSCC.

## 6.0 Other Environmental Factors

There is an additional environmental factor, i.e., boron in the coolant, that must be evaluated for the pressurized water reactors. More specifically, there is boric acid ( $H_3BO_3$ ), aside from the presence of dissolved oxygen and chloride in the Palisades CRDM environment.

Studies have been performed to examine the effects of boric acid,  $H_3BO_3$  and sodium tetraborate ( $Na_2B_4O_7$ ) on the IGSCC propensities of furnace sensitized Type 304 stainless steel in 550 °F (288 °C) 200 ppb oxygenated water. For example, constant extension rate test (CERT) "crack propagation rates" in a 100 ppb tetraborate ( $B_4O_7$ ) solution (39 ppb B) are lower than obtained in the "pure" water environment; i. e., sodium tetraborate appears to be an inhibitor to IGSCC (18), Figure 6. The CERT tests in similar acid solutions revealed that boric acid had only a slight detrimental effect on crack propagation rate, Figure 7. This latter result is most likely due to the decrease in pH rather than the presence of borate oxyanion. (It must be noted that the CERT technique is a crack initiation test and is not designed for crack growth rate studies; i.e., although CERT is excellent for ranking materials within environments, the absolute crack growth rates obtained from such a test are not valid and can be as much as three orders of magnitude higher than the experimental results.)

Studies have also been performed to examine the effects of sodium tetraborate on the IGSCC propensities of furnace sensitized Type 304 stainless steel in 550 °F (288 °C) water containing sulfate at extremely low dissolved oxygen levels (<0.5 ppb) (18). Most of the experiments were performed in water containing 10 ppm sulfate. Sodium tetraborate was added to the autoclave feedwater at anion concentrations between 1 and 1000 ppm to investigate the IGSCC response ascribable to the sulfate ion for different borate concentrations.

The results of the CERT studies indicate that a higher molar ratio of borate to sulfate generally results in higher ductility values as reflected by percent elongation and time to failure. In fact, at constant sulfate values of 10 ppm, the addition of sodium tetraborate appears beneficial, i.e., lower susceptibility, relative to furnace sensitized Type 304 stainless steel, Figure 8. This effect may be due to the competition between the “harmless” borate and the detrimental sulfate anions for surface sites available for electron transfer. This <0.5 ppb oxygen study result suggests that borate/boric acid additions to PWRs would have beneficial effects on SCC in the presence of sulfate and, therefore, perhaps chloride as well.

The mitigation of IGSCC by borate is supported by the results of uniaxial constant load studies on furnace sensitized Type 304 stainless steel at 400 °F (204 °C) in both highly oxygenated (8 ppm) and borated water (as boric acid [2,100 ppm B]) (19). Constant load times to failures were statistically compared by plotting the cumulative probability assuming the log normal distribution. The comparison at the medium (50% of cumulative probability) time to failure indicated less IGSCC susceptibility in borated water (time-to-failure was 132 hours compared to 55 hours in the pure water oxygenated environment), Figure 9. A stress dependency plot of the IGSCC propensities of furnace sensitized Type 304 stainless steel at 400 °F in both highly oxygenated (8 ppm) and borated water also demonstrated the benefits of boric acid at other applied stress levels, Figure 10.

## **7.0 Residual Stress Considerations**

The weld overlay repair has been determined to be a successful remedy for degraded piping [19]. In addition to providing a corrosion resistant, full structural reinforcement to the flawed component, the weld overlay provides a compressive residual stress on the pipe inside surface when applied to a pipe to pipe weld. This compressive residual stress is sufficient to eliminate or reduce the driving force for crack initiation and crack growth. These results have been determined in the field and confirmed by testing and analyses. There has been no incidence of crack initiation under a weld overlay or propagation into a weld overlay in more than 1,000 weld overlay repair applications in the field.

The effect of a weld overlay on the residual stress of the CRD-21 reducer configuration was analyzed using finite element methodology. The objective of this analysis was to examine the effect of the shoulder and the thick taper section of the eccentric reducer on the weld overlay residual stress field. The finite element model used was an axisymmetric model assuming the thick taper section uniformly around the circumference. It was also assumed that the residual stress on the straight side of the eccentric reducer is very similar to the residual stress from the weld overlay applied to a pipe to pipe weld. The residual stresses presented in the following paragraphs are for the azimuth angle of 180°, (i.e. the taper side of the eccentric reducer).

The predicted axial and hoop residual stresses are presented in Figure 11, at the crack location below the weld between the CRDM housing and the eccentric reducer. This is the location where the largest circumferential crack was detected. It is also in the region where the residual stress is most unfavorable due to the presence of the shoulder area and the changes in the geometric configuration. Using the stress profiles in this location would provide a conservative upper bound estimate of the driving force for crack propagation. This less favorable residual

stress is limited to locations near the 180° azimuth since the 0° azimuth represents a straight pipe-to-pipe that will produce the more favorable residual stress distribution expected for pipe-to-pipe configurations. It is also noteworthy that these residual stress distributions with the weld overlay applied reduce the driving force for crack growth compared to the as welded component for all azimuthal locations.

Stress intensity factors associated with different crack geometries were calculated using the predicted residual stress profiles presented in Figure 11, combined with pressure and seismic stresses. The through-wall residual stresses were curve-fit using a 3<sup>rd</sup> order polynomial. The hoop and axial stresses due to pressure were 8.4 ksi and 4.2 ksi, respectively, using the equation for a thin wall cylinder, accounting for the increase in wall thickness due to the weld overlay. The seismic stress was 3.4 ksi. Both pressure and seismic stresses were assumed to be constant through-wall. The crack model used was for a full circumferential crack and an elliptical axial crack with crack aspect ratios of  $l/a = 5$  and 2. The results of the metallurgical examination of the cracked CRDM at Palisades revealed a crack aspect ratio of  $l/a = 4$ . The results from  $l/a = 2$  and  $l/a = 5$  were interpolated to obtain the results for  $l/a = 4$  corresponding to the field observed crack aspect ratio.

The stress intensity factors for the circumferential crack due to residual stress are presented in Figure 12. The stress intensity factors for the circumferential crack due to pressure and seismic loads are presented in Figure 13. The total stress intensity factor due to the combination of residual stress, pressure and seismic loadings is presented in Figure 14. It can be seen that the residual stress is beneficial when combined with the operating stresses, in reducing the driving force for crack growth. The results demonstrate that the stress intensity factor is less than 20 ksi√in for a circumferential crack through the original wall thickness.

The stress intensity factors for the elliptical axial crack due to the weld overlay through wall hoop residual stress (Figure 11) are shown in Figure 15 for crack aspect ratios,  $l/a = 5$  and 2. The stress intensity factors for the elliptical axial crack due to the hoop pressure stress are shown in Figure 16. The total stress intensity factors due to pressure and weld overlay residual hoop stresses for  $l/a = 5$  and  $l/a = 2$  and interpolated to  $l/a = 4$  are presented in Figure 17. The results demonstrate that the stress intensity factor remains less than 25 ksi√in for an axial crack through the original wall thickness.

Bounding TGSCC growth data are presented in Figure 18 for austenitic stainless steels in a concentrated sodium chloride (22%) solution at 221 °F (105°C) (17). This figure shows that the  $K_{ISCC}$  threshold is about 18 ksi√in (20 MPa√m) in the concentrated sodium chloride solution. These very conservative results suggest that little or no crack growth is expected either in the wrought 347 SS or into the overlay for the calculated stress intensity factors for circumferential or for axial flaws.

In addition, it should be noted that the stress intensity factor calculation presented herein is for the 180° azimuth location. As the circumferential crack extends beyond this location, and toward the 0° azimuth, the residual stress pattern in both axial and hoop direction would be much more compressive as discussed above, thus providing additional conservatism to the analysis.

## 8.0 Conclusions

The available data, modeling and residual stress calculations produced the following conclusions:

1. Based on material and environmental FOI considerations, the initiation of environmentally assisted cracking, i.e., CSCC, IGSCC or TGSCC, in the planned Type 309L stainless steel weld overlay is unlikely.
2. Based on material and environmental modeling FOI considerations, the propagation of environmentally assisted cracking, in the planned Type 309L stainless steel weld overlay would be more than one order of magnitude slower than in Type 304 stainless steel.
3. The application of weld overlay provides favorable through-wall residual stress profiles that reduce the driving force for environmentally assisted cracking propagation either in the Type 347 stainless steel or into the weld overlay once the weld overlay is applied.

The synergistic combination of the above factors clearly suggest that the planned Type 309L stainless steel weld overlay can be considered as a permanent repair for the CRDMs at Palisades. The weld overlay application approach for the CRDMs at Palisades is consistent with the NRC philosophy of the application of dual remedial measures for the mitigation of SCC. That is, the Type 309L stainless steel weld overlay clearly addresses two of the three required parameters for SCC, i.e., susceptible material and tensile stress.

## 9.0 References

1. D. R. McIntyre, "Experience Survey Stress Corrosion Cracking of Austenitic Stainless Steel in Water, MTI Publication No. 27, February 1987.
2. B. M. Gordon, "The Effect of Chloride and Oxygen on the Stress Corrosion Cracking of Stainless Steel: Review of Literature," *Materials Performance*, Vol. 19, No. 4, April 1980.
3. A. J. Sedriks, Corrosion of Stainless Steels, John Wiley and Sons, New York, NY, 1979.
4. U. Steinsmo and J. M. Drugli, "Assessment of Susceptibility to Chloride Stress Corrosion Cracking of Highly Alloyed Stainless Steels. Part 1: Drop Evaporation Test Method," paper #193 presented at Corrosion 97, New Orleans, LA, March 9-14, 1997.
5. R. L. Cowan and G. M. Gordon, "Intergranular Stress Corrosion Cracking and Grain Boundary Composition of Fe-Ni-Cr Alloys, NEDO-12399, 73 NED 106, Class 1, September 1973.
6. "BWR Vessel and Internals Project, Technical Basis for Inspection Relief for BWR Internal Components with Hydrogen Injection (BWRVIP-62)," EPRI TR-108705, Palo Alto, CA, December 1998.

7. G. C. Bodine, Jr. and C. H. Sump, "Development of Wrought Austenitic-Ferritic Stress Corrosion Resistant Alloys with Less than 40% Ferrite for Pipe and Tube," paper #137 presented at Corrosion 1977, NACE, San Francisco, CA, March 14-18, 1977.
8. B. Lisowyj, "Evaluation of Cracking in Type 348 Stainless Steel Control Element Drive Mechanism Housing," paper presented at the Sixth International Symposium on Environmental Degradation of Materials in Nuclear Power Systems – Water Reactors, San Diego, CA, August 1-5, 1993, published in proceeding of same, TMS, Warrendale, PA, 1993, p. 343.
9. W. J. Shack, et al., "Environmentally Assisted Cracking in Light Water Reactors," Semi-annual Report, Argonne National Laboratory, NUREG/CR-4667, ANL-89/10, Vol. 6, October 1987-March 1988, p. 14.
10. W. L. Clarke and G. M. Gordon, "Investigation of Stress Corrosion Cracking Susceptibility of Fe-Ni-Cr Alloys in Nuclear Reactor Water Environments," Corrosion, Vol. 20, No. 1, January 1973, p. 1.
11. F. P. Ford private communication with B. M. Gordon, August 2, 2001.
12. P. L. Andresen, "Effects of Specific Anionic Impurities on Environmental Cracking of Austenitic Materials in 288°C Water," paper presented at the Fifth International Symposium on Environmental Degradation of Materials in Nuclear Power Systems - Water Reactors, ANS, 1992, p. 209-218. F. P. Ford, "Mechanisms of Environmental Cracking in Systems Peculiar to the Power Generation Industry," EPRI NP-2589, Palo Alto, CA, September 1982.
13. F. P. Ford, "Mechanisms of Environmental Cracking in Systems Peculiar to the Power Generation Industry," EPRI NP-2589, Palo Alto, CA, September 1982.
14. F. P. Ford, et al., "Environmentally-Controlled Cracking of Stainless and Low-Alloy Steels in Light-Water Reactors," EPRI NP-5064S, Palo Alto, CA, February 1987.
15. F. P. Ford and D. Weinstein, "The Effect of Improved Water Chemistry on Corrosion Cracking of BWR Piping," EPRI NP-6585, , Palo Alto, CA, December 1989.
16. P. L. Andresen, "Stress Corrosion Monitoring and Component Life Prediction in BWRs," EPRI TR-1000399, Palo Alto, CA, March 1992.
17. R. C. Cipolla and N. G. Cofie, "Technical Basis for Temporary Acceptance of Flaws in Moderate Energy Piping as Prescribed in Code Case N-513," Proceedings of Pressure Vessel Piping Conference NRC/ASME BPVC Section XI Symposium, Atlanta, GA, 2001.
18. W. J. Shack, et al., "Environmentally Assisted Cracking in Light Water Reactors: Annual Report October 1983 - September 1984," NUREG/CR-4287, ANL-85-33, June 1985.

19. T. Tsuruta and S.Okamoto, "Stress Corrosion Cracking of Sensitized Austenitic Stainless Steel in High Temperature Water," Corrosion, Vol. 48, No. 6, June 1992, p. 518.
20. "Assessment of Remedies for Degraded Piping," EPRI NP-5881-LD, Project T302-1, June 1988.

**Table 1. Chromium Equivalents for Types 309L and 2205 Stainless Steel (3)**

<b>Element</b>	<b>304</b>	<b>309L (ASME)</b>	<b>2205</b>
C	0.08	0.03	0.030
Mn	2.00	1.0-2.5	2.0
Si	1.00	0.30-0.65	1.0
Cr	18.0-20.0	23.0-25.0	21.0-23.0
Ni	8.0-10.5	12.0-14.0	4.5-6.5
Mo		0.75	2.50-3.5
Cu		0.75	
N	0.10		0.08-0.20
Cr Equivalent	21	26.1	28.5

$$Cr_{eq} = \%Cr + 2(\%Si) + 1.5(\%Mo) + 5(\%V) + 5.5(\%Al) + 1.75(\%Nb) + 1.5(\%Ti) + 0.75(\%W) \quad (3)$$

Figure 1. The Effects of Oxygen and Chloride on the Initiation of SCC of Austenitic Stainless Steel in High-Temperature Water (2)

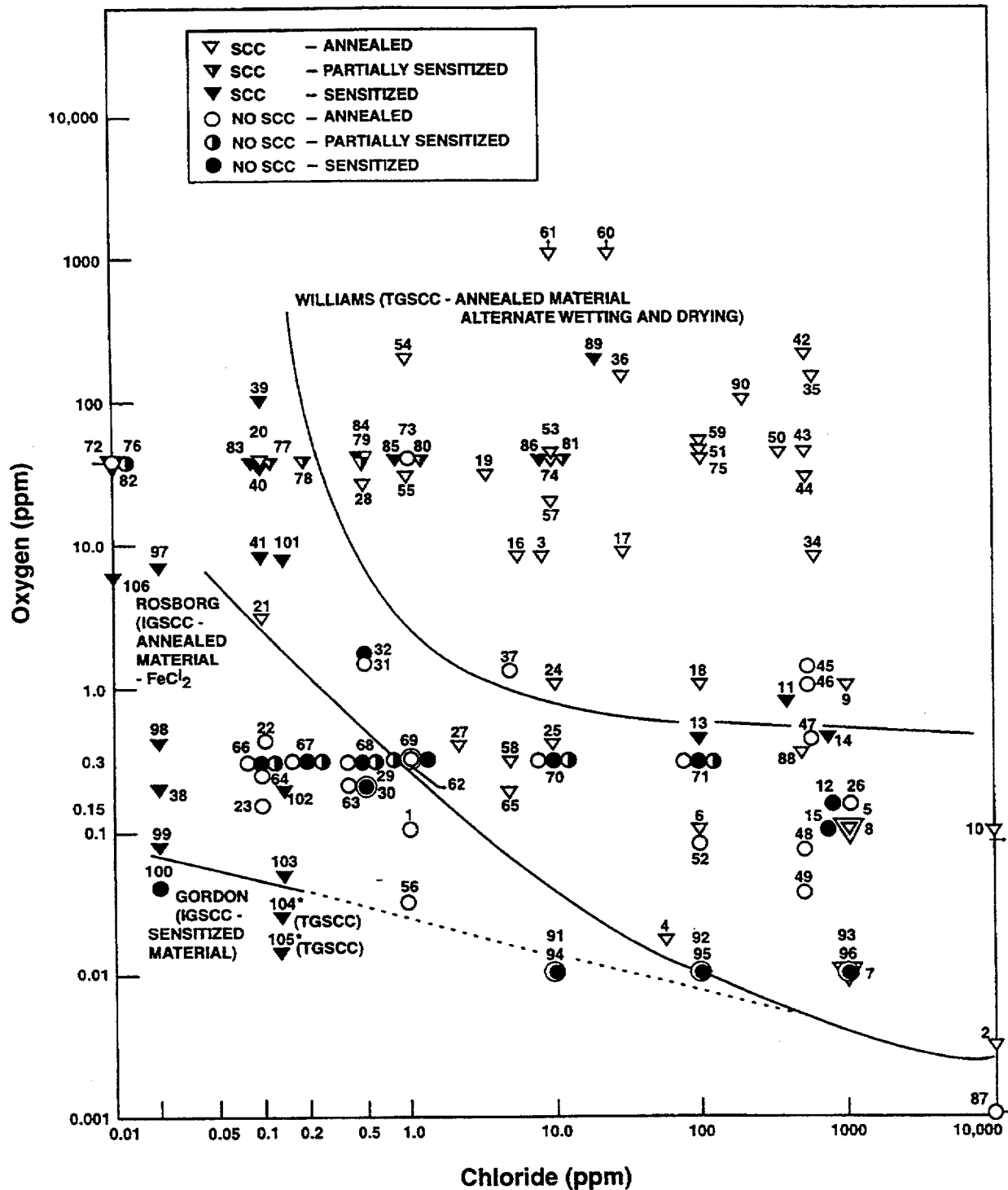


Figure 2. Relative CSCC Resistance of Solution Annealed Type 304 Stainless Steel Compared to Duplex Stainless Steel (1)

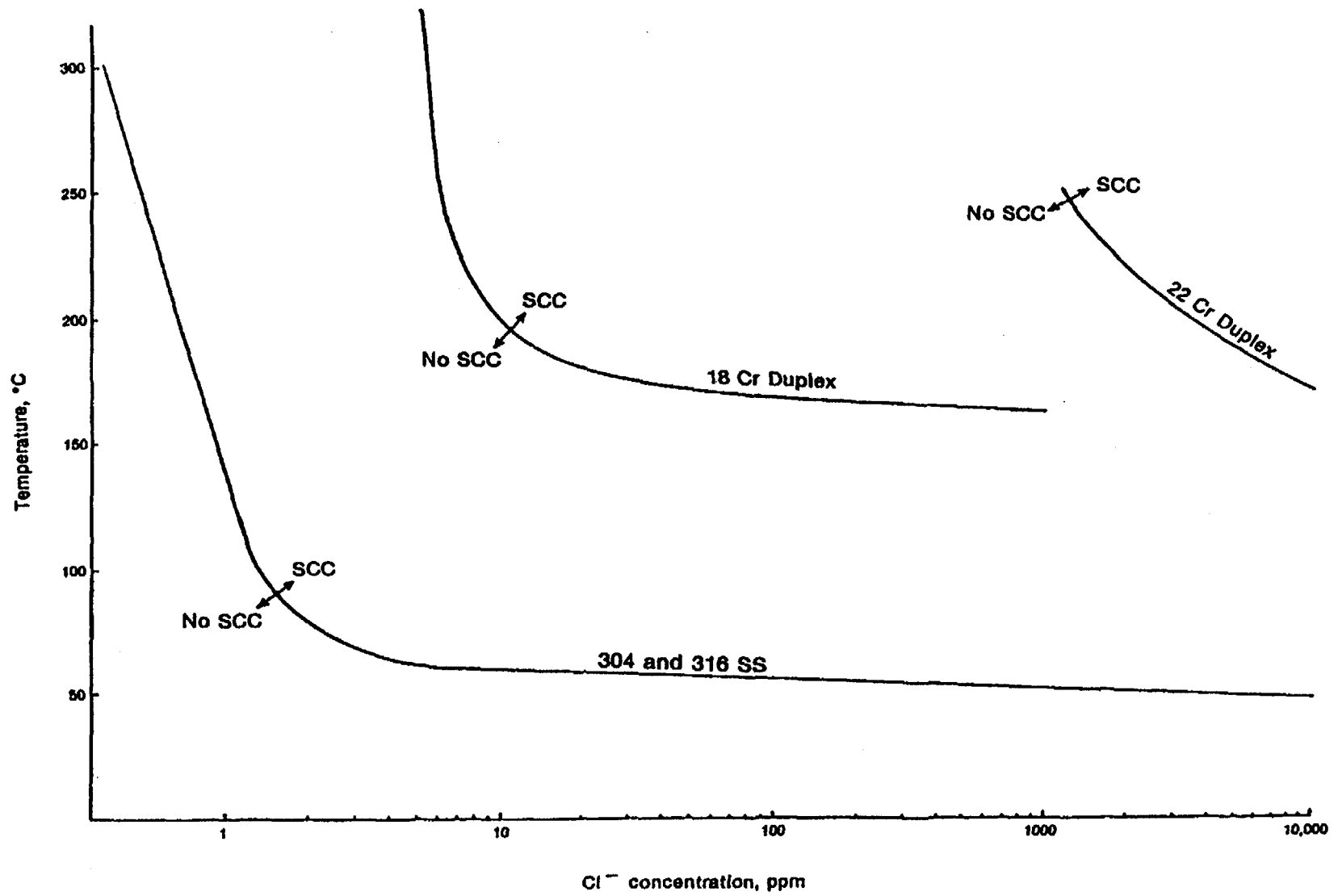


Figure 3. CSCC in Oxygenated Neutral Chloride Solutions (4)

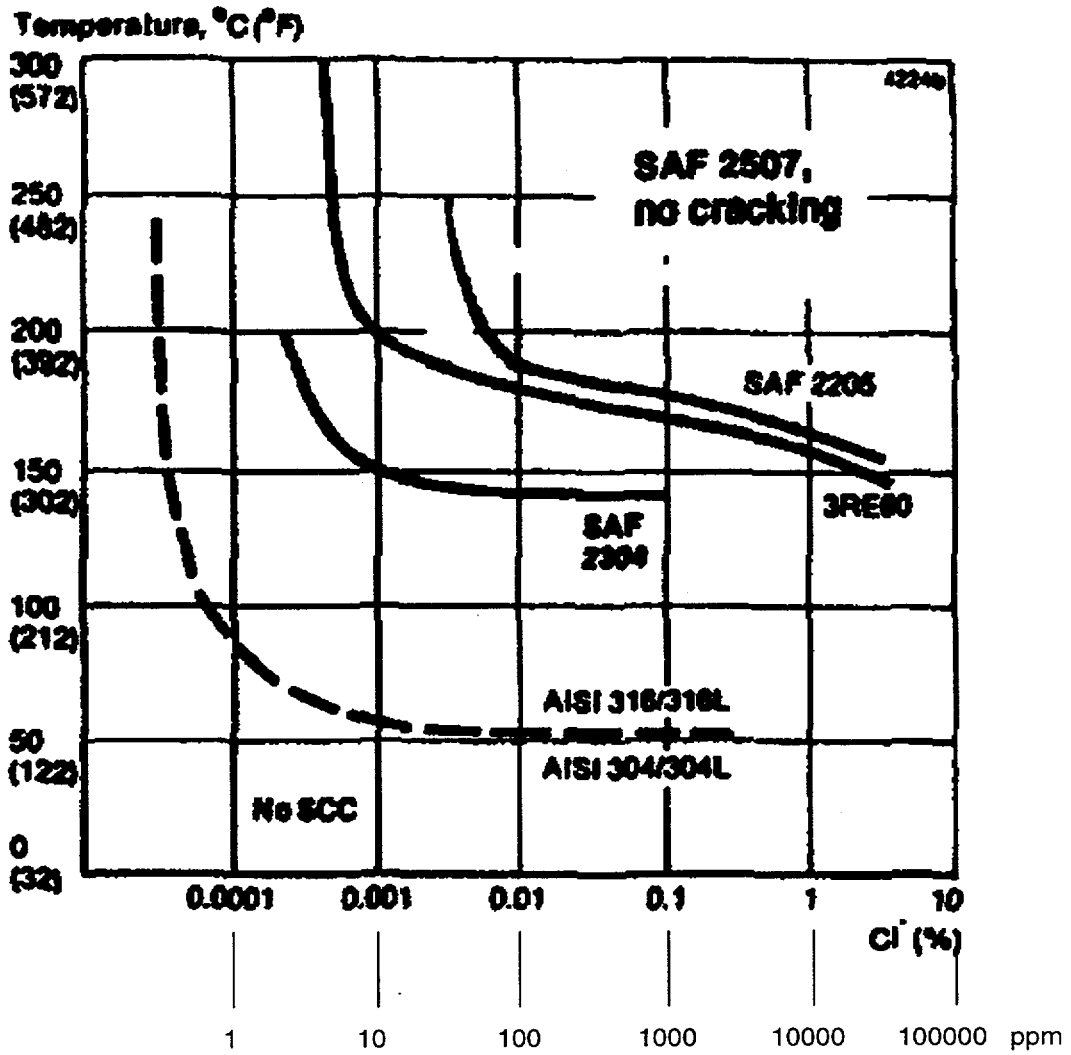
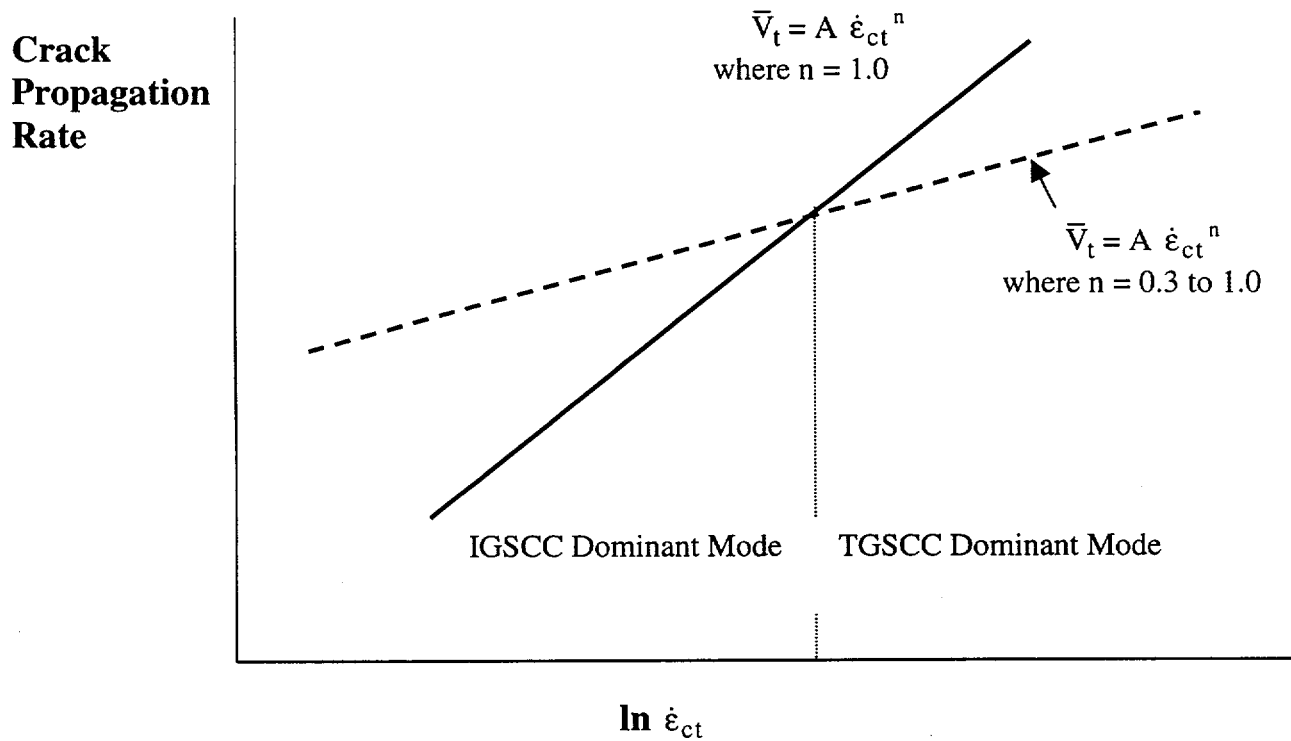
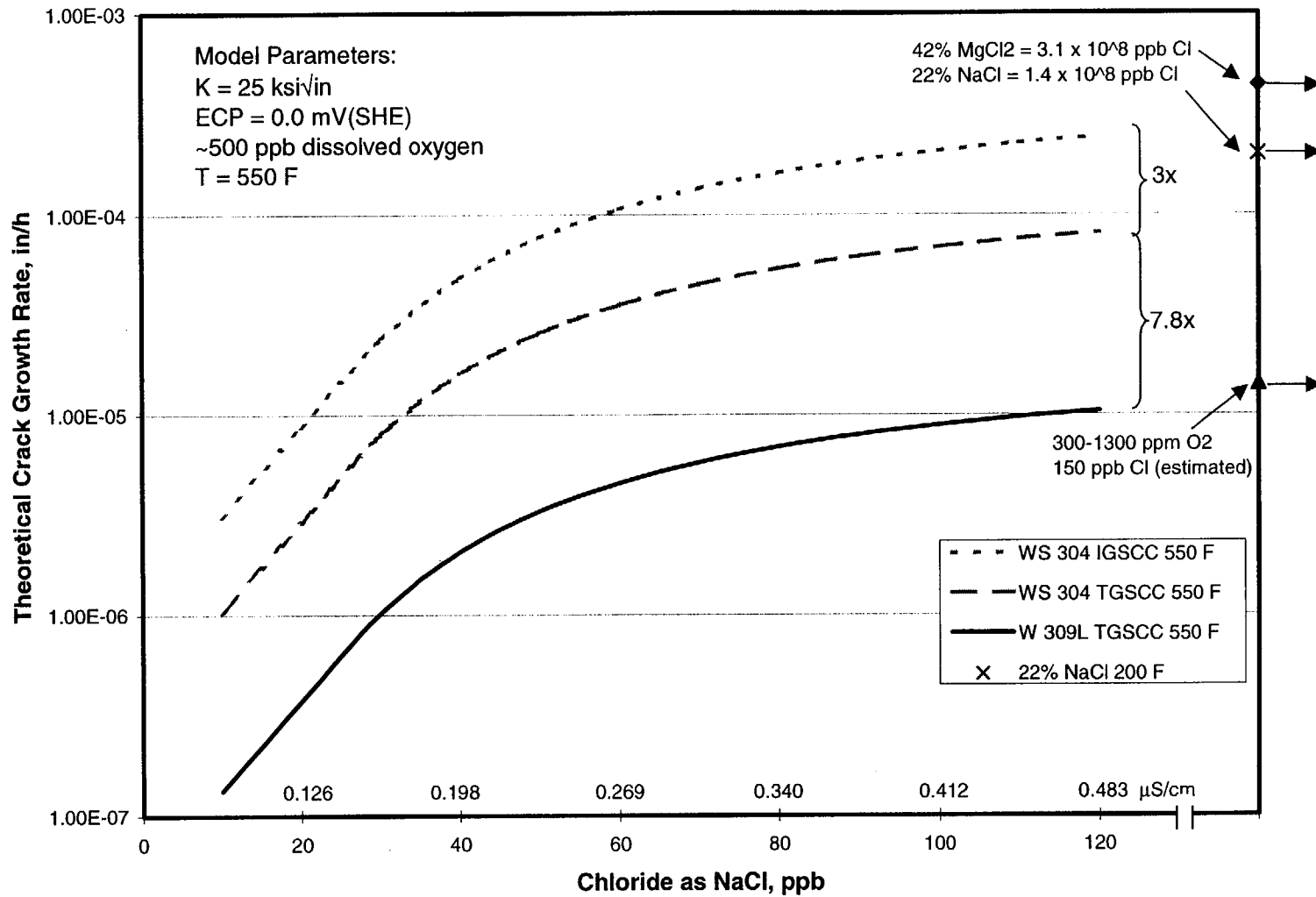


Figure 4. Schematic of Crack Propagation Rate versus Strain Rate for IGSCC and TGSCC in the Stainless Steel – Water System (11)



**Figure 5. Theoretical Predictions of the Relative Crack Growth Rates for Types 304 and 309L Stainless Steel based on the Film Rupture/Slip Oxidation Model**



Structural Integrity Associates, Inc.

**Figure 6. Effect of Various Sodium Salts on the CERT “Crack Growth Rate” of Furnace Sensitized Type 304 Stainless Steel (18)**

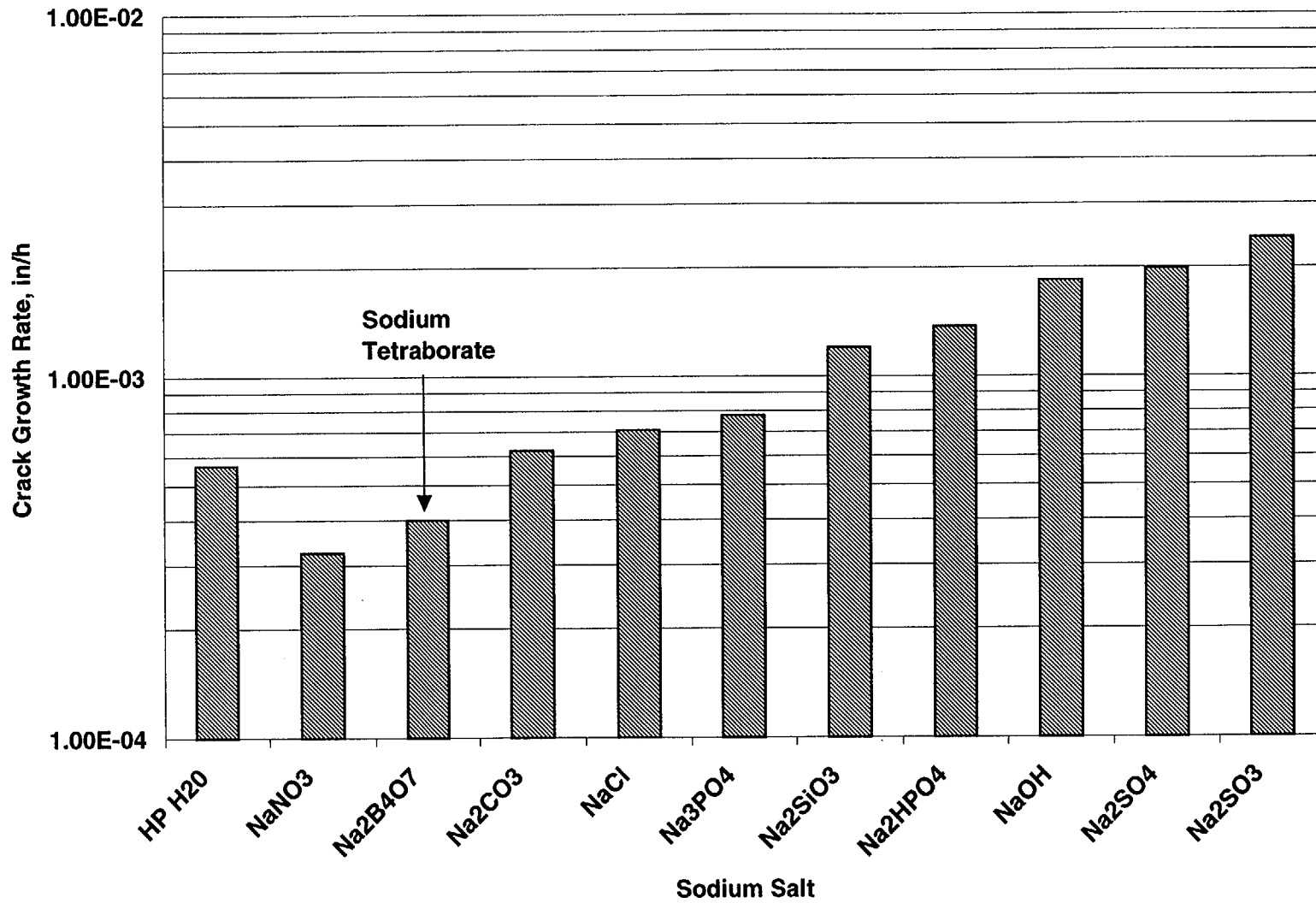
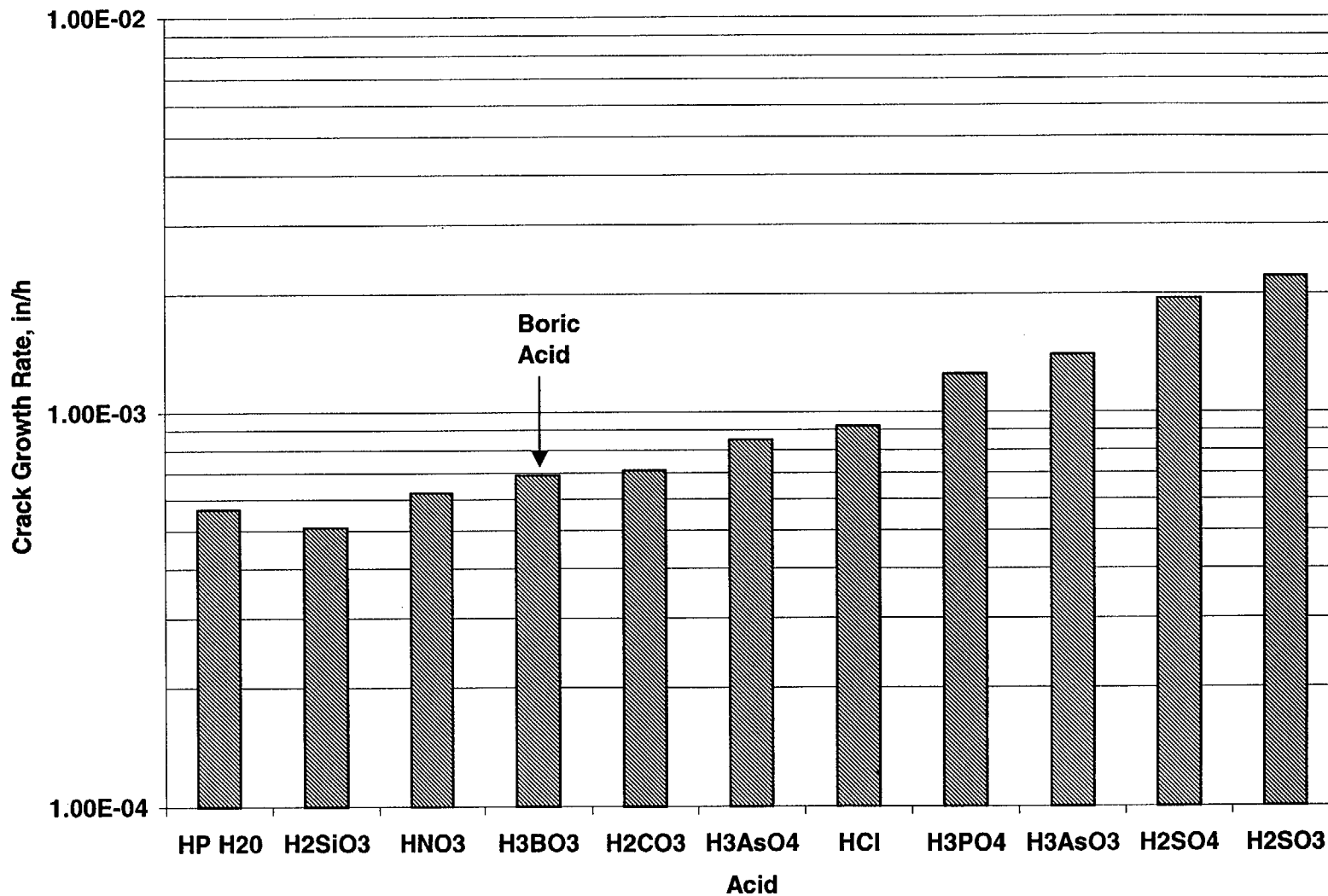


Figure 7. Effect of Various Acids on the CERT "Crack Growth Rate" of Furnace Sensitized Type 304 Stainless Steel (18)



Structural Integrity Associates, Inc.

**Figure 8: Influence of Borate to Sulfate Molar Ratio on CERT Ductility as Time to Failure ( $T_f$ ) and Percent Elongation for Furnace Sensitized Type 304 Stainless Steel in Deaerated Water (18)**

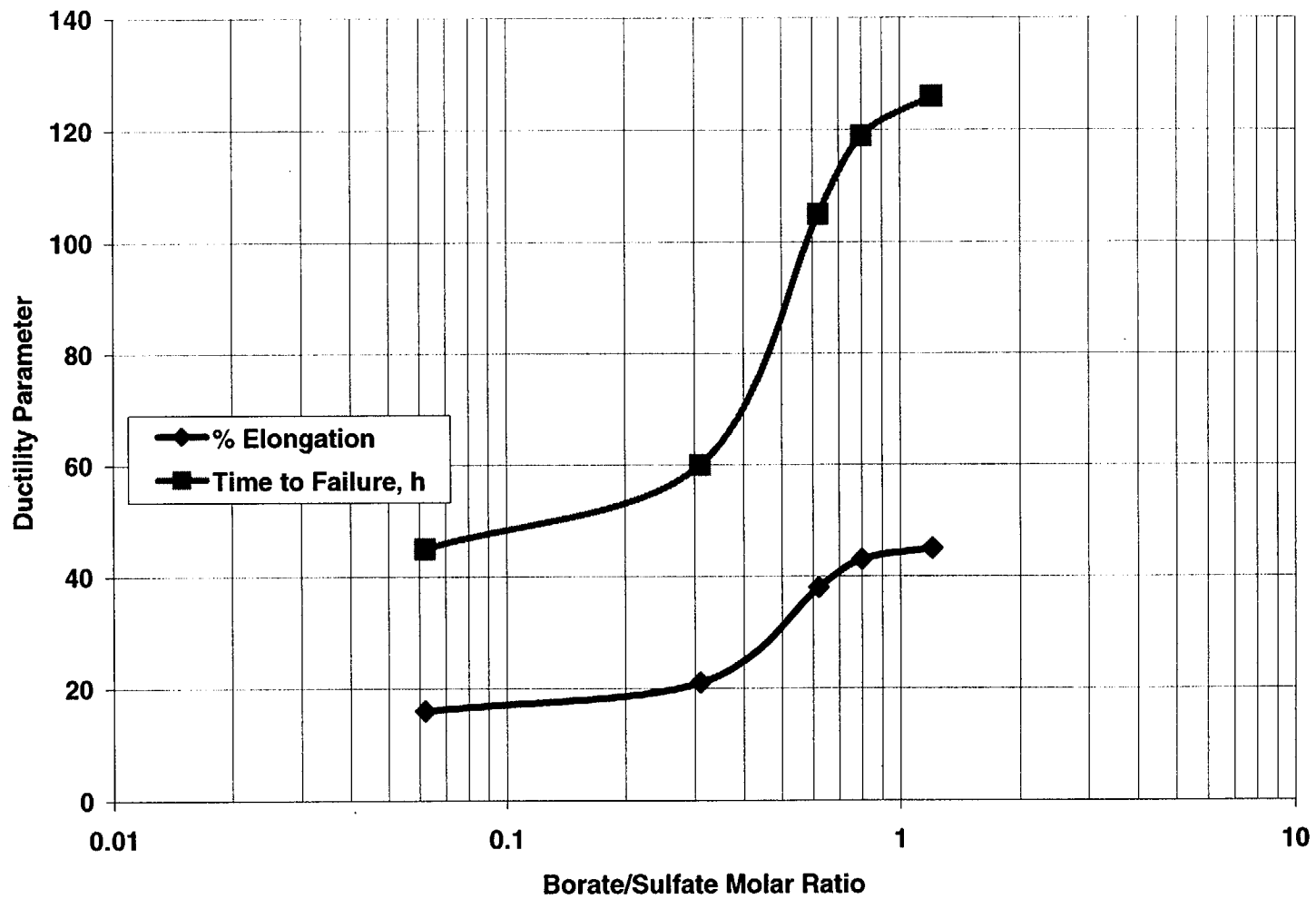


Figure 9. Comparison of Time-to-Failure in Oxygenated High-Purity Water and Borated Water for Furnace Sensitized Type 304 Stainless Steel at 50 ksi and 464 °F (19)

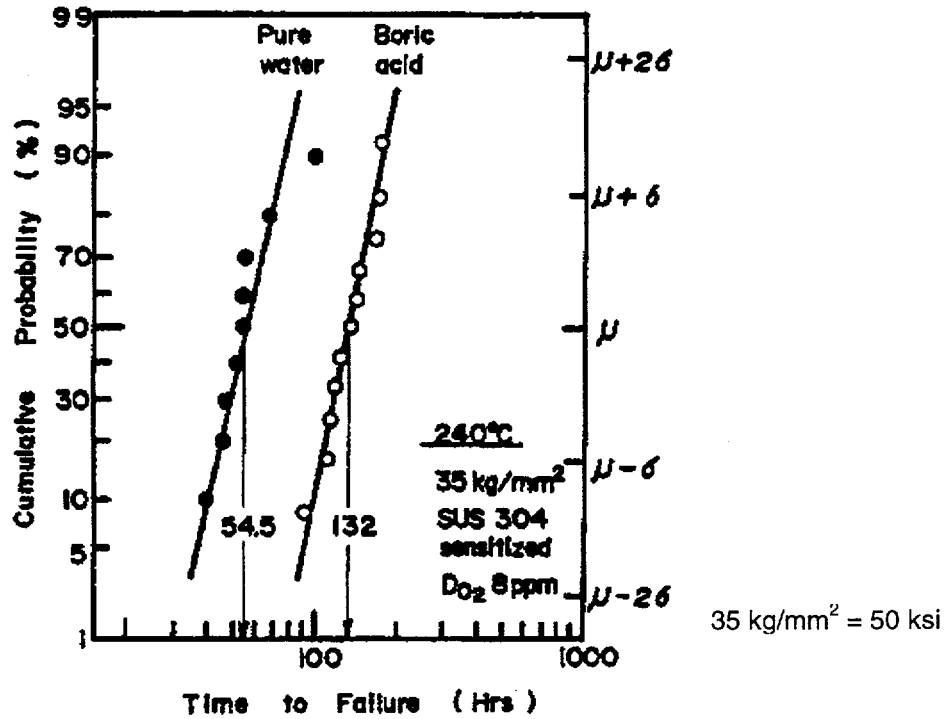


Figure 10. Uncreviced Uniaxial Constant Load Test Results in Oxygenated High-Purity Water and Borated Water for Furnace Sensitized Type 304 Stainless Steel at 464 °F (19)

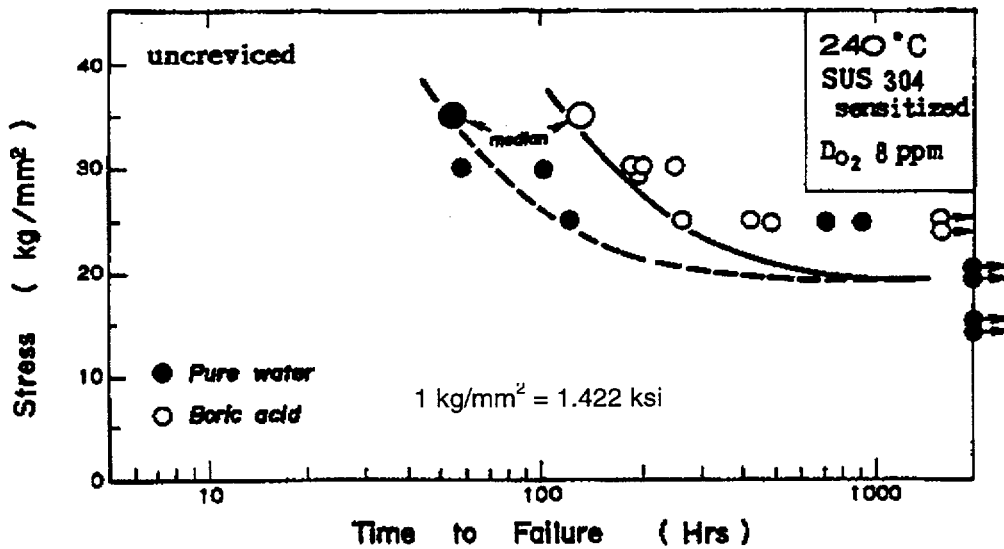


Figure 11. Through-Wall Overlay Residual Stress Profile

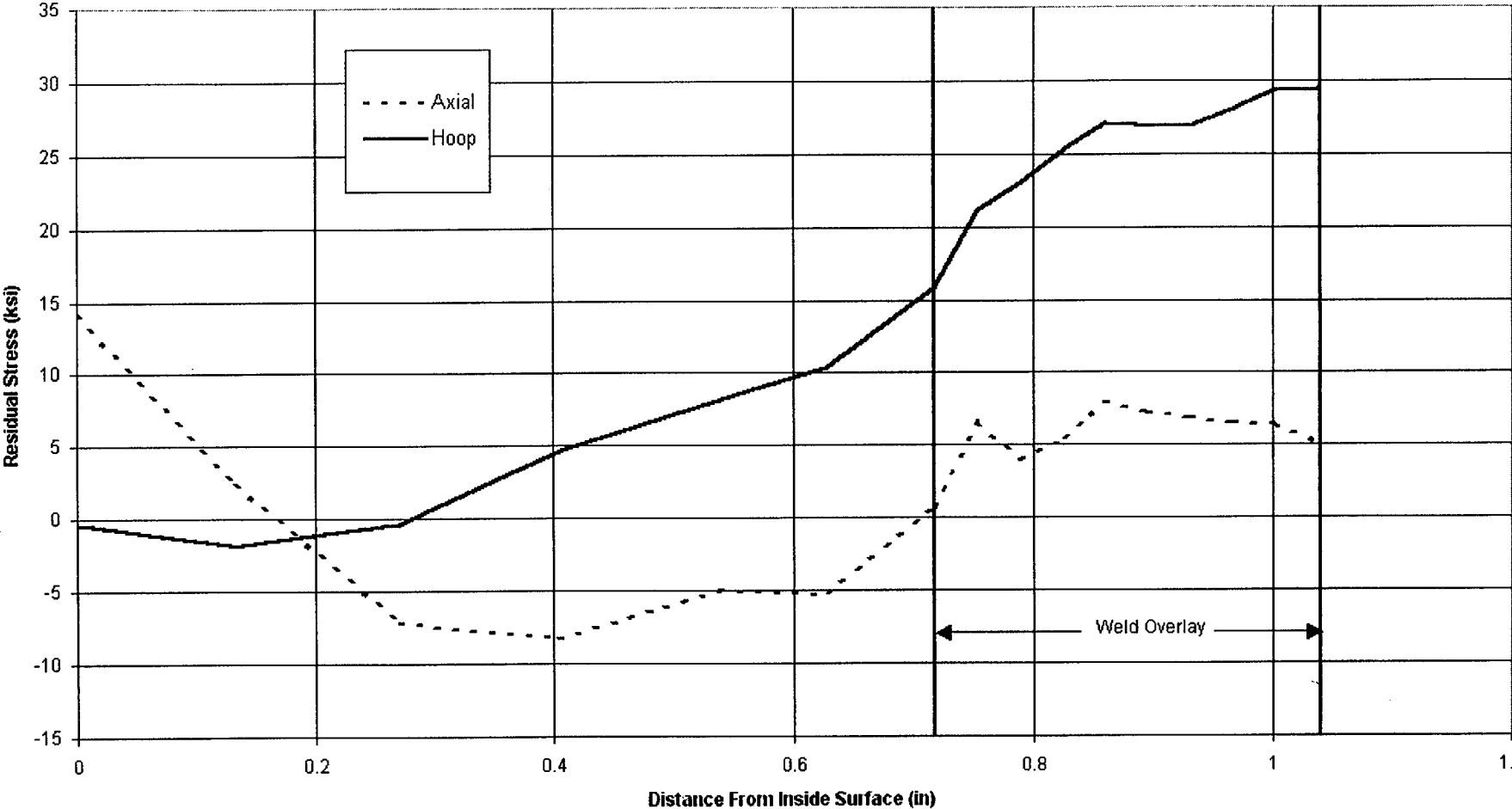
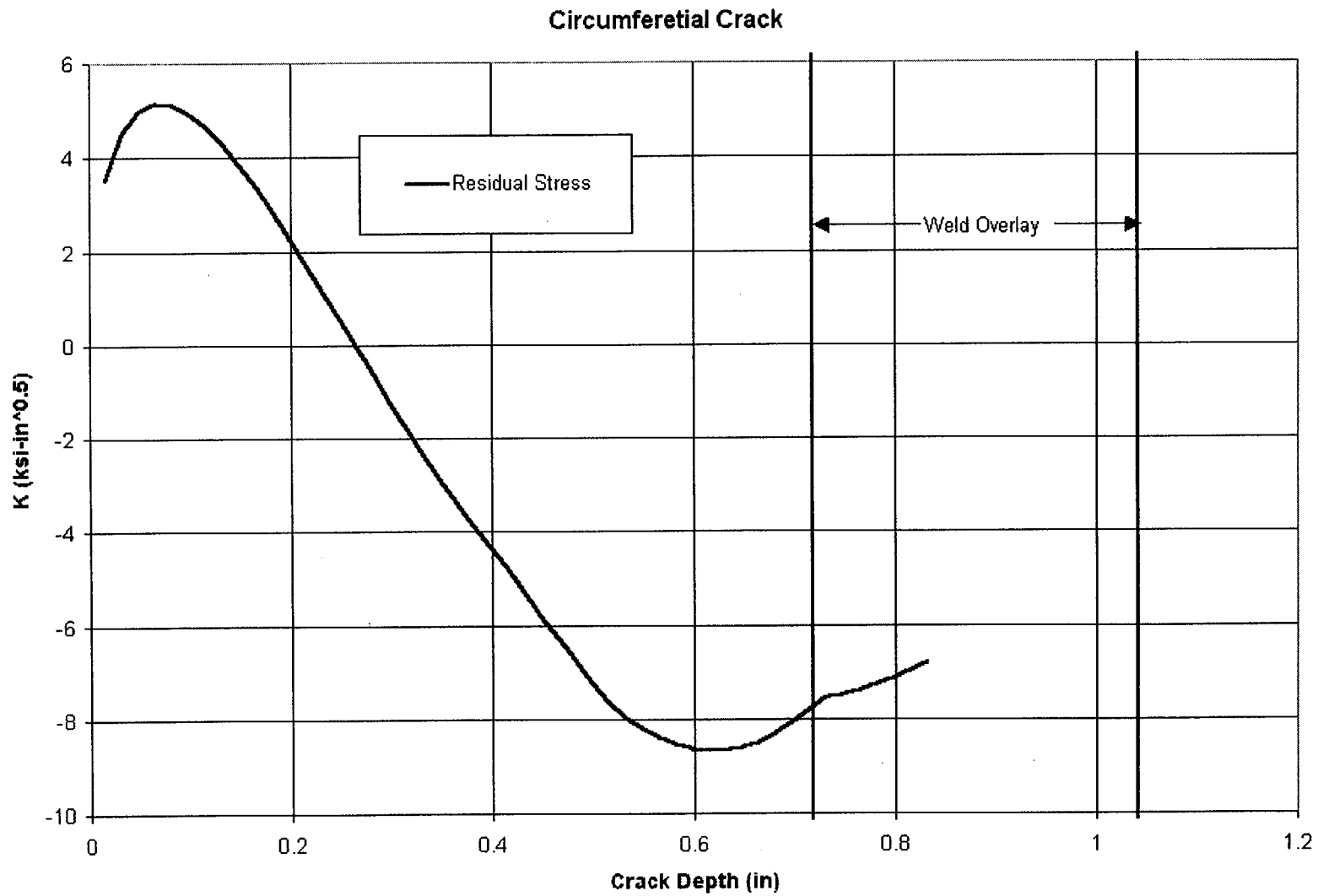


Figure 12. Stress Intensity Factors for Circumferential Crack



**Figure 13. Stress Intensity Factors due to Overlay Pressure and Seismic Stress, Circumferential Crack**

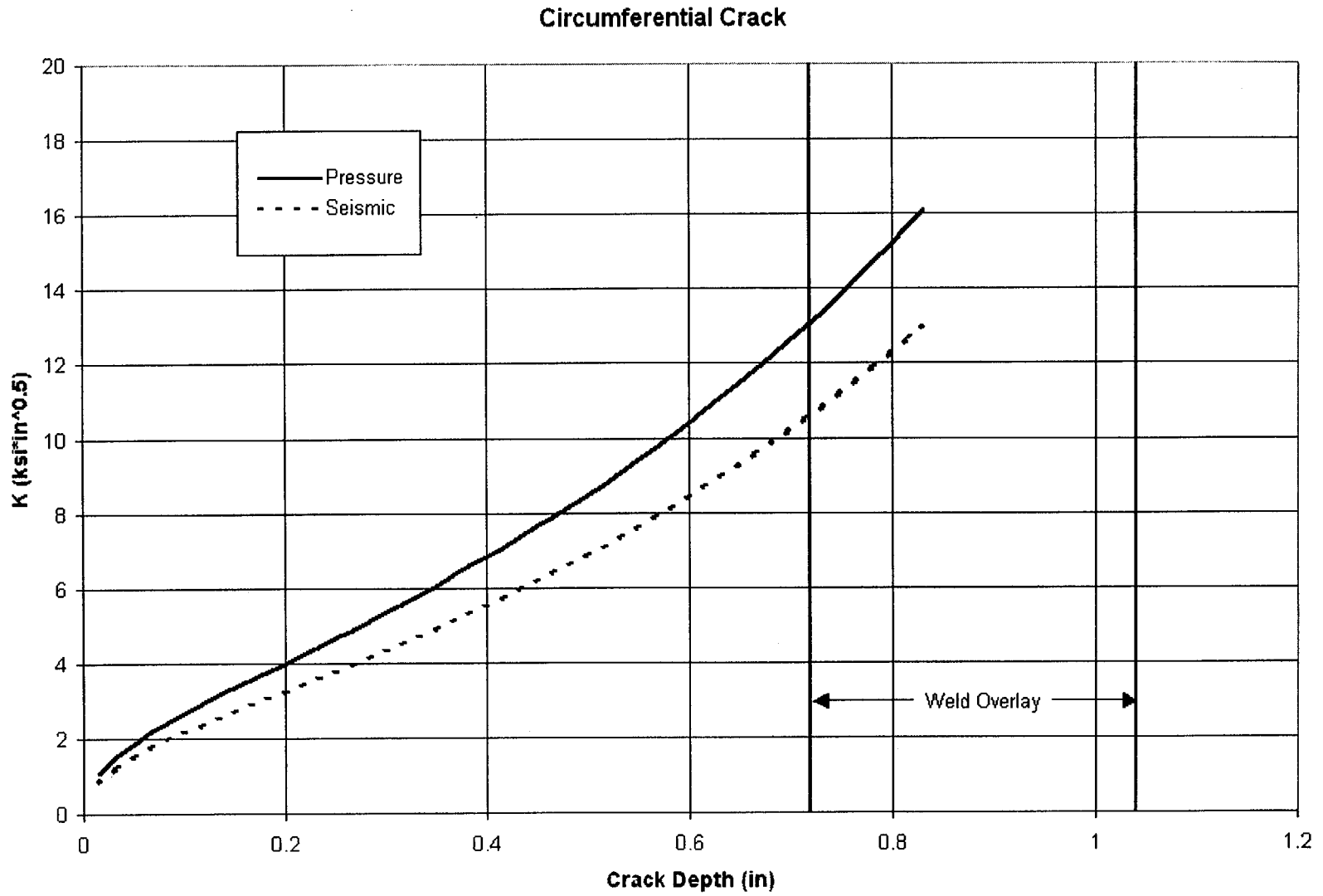


Figure 14. Stress Intensity Factor due to Overlay Residual, Pressure and Seismic Stresses

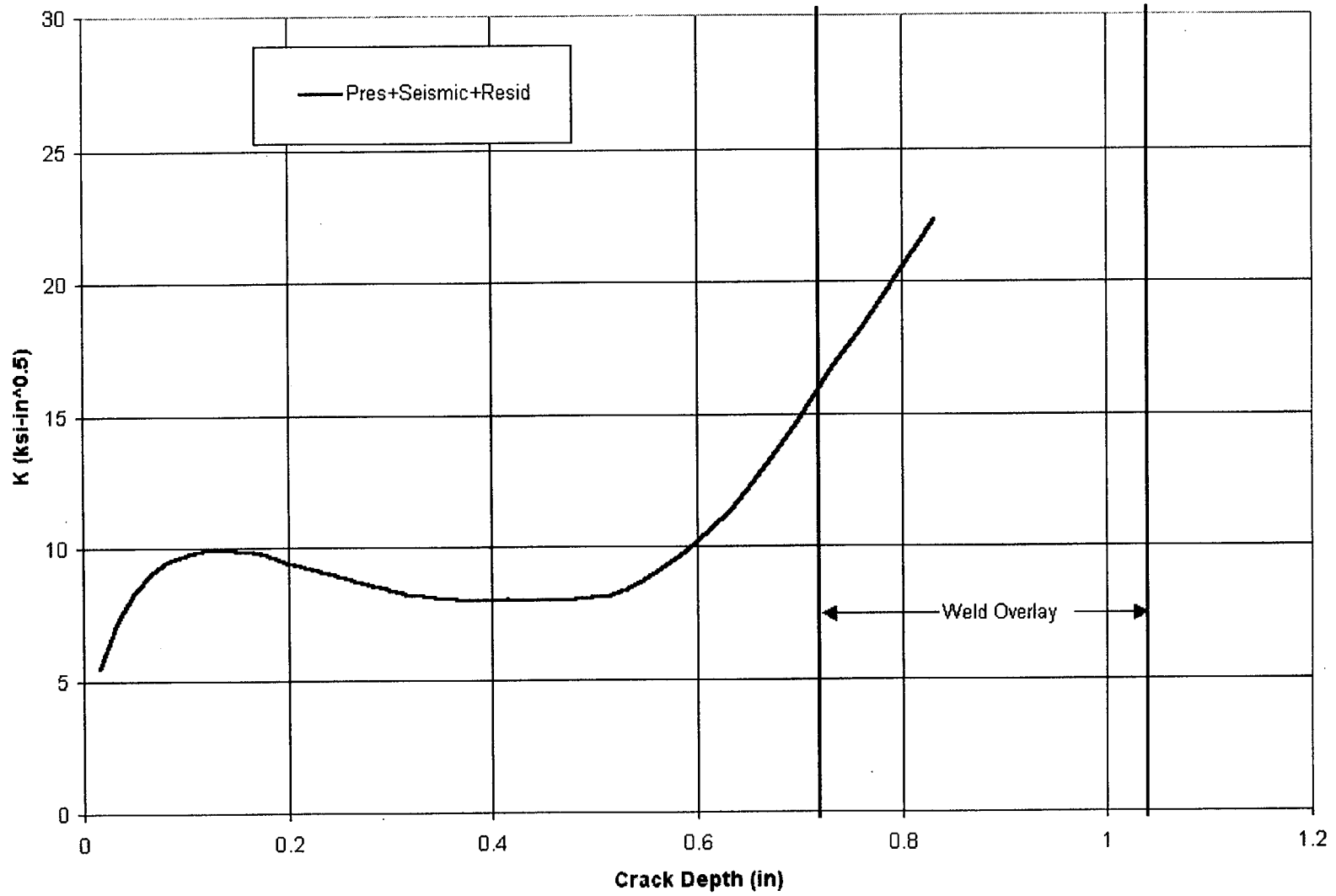
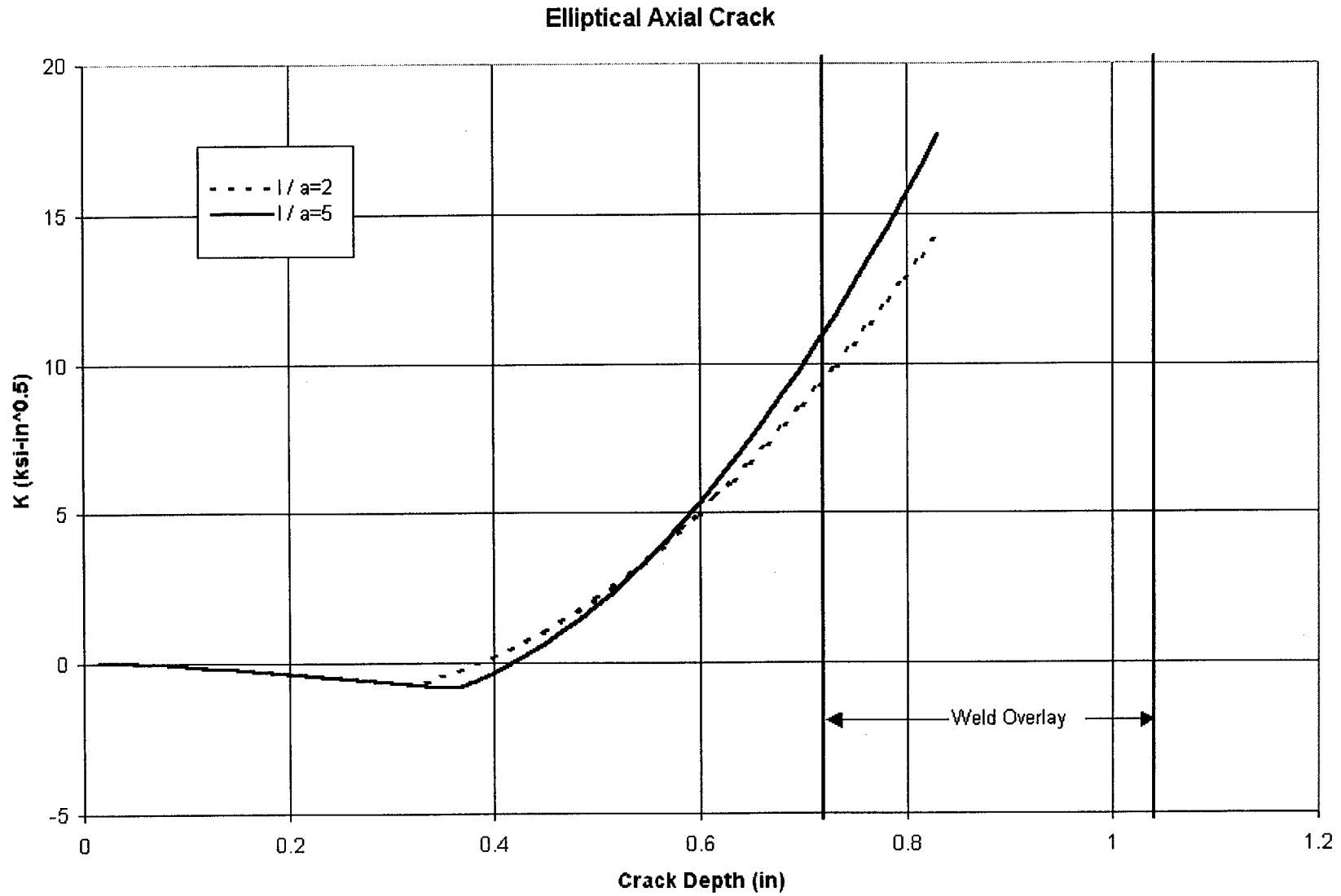
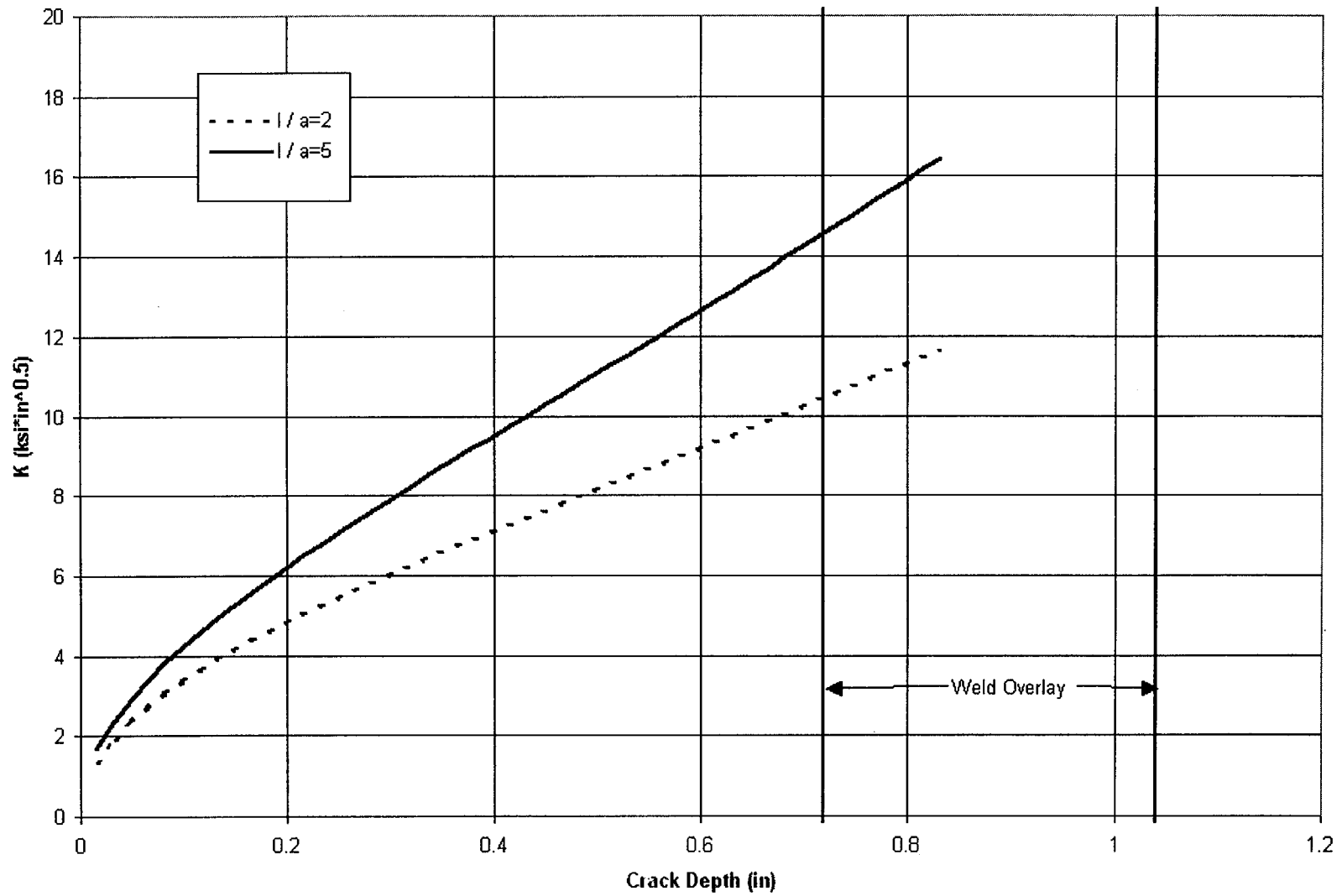


Figure 15 Stress Intensity Factor due to Overlay Residual Stress, Axial Crack



**Figure 16 Stress Intensity Factor due to Pressure Stress for Elliptical Axial Cracks**



**Figure 17 Stress Intensity Factor for Axial Cracks due to Overlay Residual and Pressure Stresses**

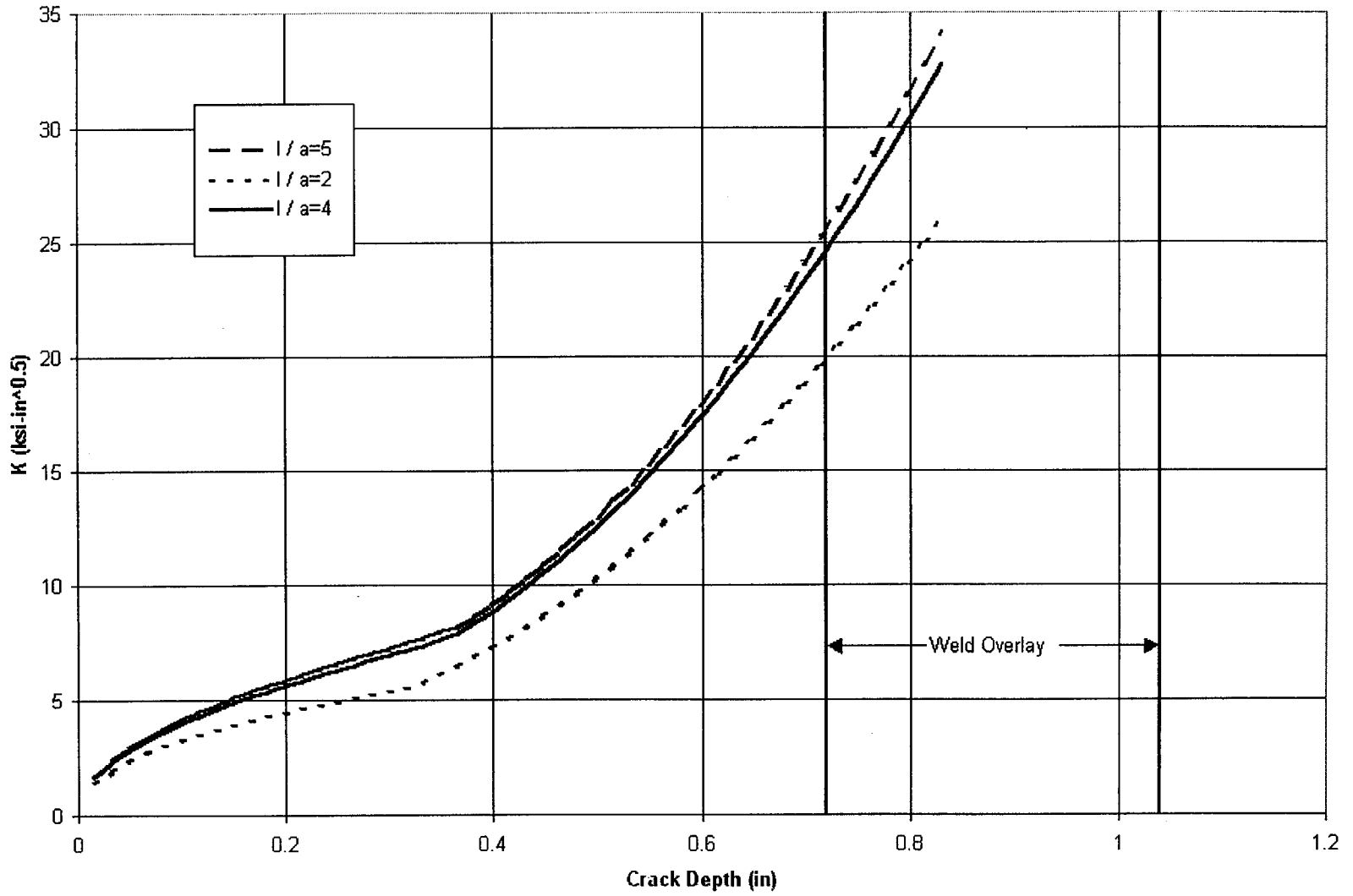


Figure 18. Effect of Stress Intensity Factor on Growth Rates in Austenitic Stainless Steels in Sodium Chloride and Magnesium Chloride Solutions (17)

